crystals

MDPI

Article

[5,5]-Fused Anhydride, Thioanhydride, and Imide Derivatives of Cyclopentadienyl Complexes: Electronic Effects of $Mn(CO)_3$ and Ru(Cp*) Fragments

Uttam R. Pokharel [1,*], Sean Parkin [2] and John P. Selegue [2]

[1] Department of Mathematical, Applied & Physical Sciences, University of Houston Clear-Lake, Houston, TX 77058, USA
[2] Department of Chemistry, University of Kentucky, Lexington, KY 40506, USA; s.parkin@uky.edu (S.P.); selegue@uky.edu (J.P.S.)
* Correspondence: pokharel@uhcl.edu

Abstract

A new approach to 5,5-fused heterocyclic derivatives of cyclopentadienylmanganese tricarbonyl and pentamethylruthenocene is presented. 1,2-Dicarbophenoxycyclopentadienyl complexes of manganese and ruthenium were hydrolyzed to 1,2-dicarboxylic acids. Oxalyl chloride converted the acids to chlorocarbonyls, which reacted with bis(trimethylsilyl)sulfide to give the cyclopentadienyl-fused thioanhydrides. Alternatively, dehydration of the diacids with trifluoroacetic anhydride closed the diacids to cyclopentadienyl-fused anhydrides. Treatment of the anhydrides with *p*-toluidine followed by oxalyl chloride led to cyclopentadienyl-fused carboxylic imides. This approach enables direct comparison of electron-deficient $Mn(CO)_3$ and electron-rich Ru(Cp*) coordination environments on the 5,5-fused heterocycles. Spectroscopic data reveal systematic downfield NMR shifts and higher infrared carbonyl stretching frequencies for the manganese complexes, consistent with lower electron density in the $Mn(CO)_3$ compared to Ru(Cp*). Crystallographic analyses confirm that heterocycle fusion occurs without significant perturbation of the metal–cyclopentadienyl geometry. Comparative analysis across the series demonstrates that metal-dependent effects are primarily electronic rather than structural, with the $Mn(CO)_3$ and Ru(Cp*) fragments modulating electron distribution within the fused ligand framework.

Keywords: cyclopentadienyl complexes; manganese tricarbonyl; ruthenocene; fused heterocycles; thioanhydrides; imides; organometallic structure; metal–ligand electronic effects

Check for updates

Academic Editors: Nikolina Filipović, Tomislav Balić and Anamarija Stanković

Received: 9 June 2026
Revised: 22 June 2026
Accepted: 22 June 2026
Published: 24 June 2026

Copyright: © 2026 by the authors. Licensee MDPI, Basel, Switzerland. This article is an open access article distributed under the terms and conditions of the Creative Commons Attribution (CC BY) license.

1. Introduction

Cyclopentadienyl (Cp) complexes are one of the most extensively studied classes of organometallic compounds due to their structural stability, rich substitution chemistry, and tunable electronic properties [1,2]. Functionalization of Cp ligands provides a powerful strategy for modulating metal–ligand interactions and tuning the electronic properties of η^5-coordinated systems [3,4]. Recent studies have further demonstrated the diverse reactivity and electronically adaptive behavior of Cp ligands, including their participation in ring-activation processes and proton-coupled transformations [5]. In particular, selective substitution on the Cp ring enables access to tailored ligand environments that can support more complex architectures, including annulated and fused frameworks [6]. 1,2-Functionalization strategies are particularly attractive because they enable intramolecular cyclization into fused heterocyclic architectures.

1,2-Dicarboxy-functionalized cyclopentadienyl ligands and related diesters have been explored as synthetically accessible and structurally versatile systems. Complexes bearing adjacent ester or carboxy substituents have been reported for a range of transition metals, including manganese, molybdenum, rhenium, and technetium, demonstrating the generality of this ligand class and its accessibility across different coordination environments [7–9]. Related ferrocene derivatives further show that 1,2-dicarboxylate functionality can be transformed into cyclic anhydrides and other condensed structures, suggesting the potential of these systems as precursors for heterocycle formation [10–12].

Our group developed synthetic methods to functionalize the cyclopentadienyl ring with 1,2-diacyl substituents, which serve as precursors for the construction of fused heterocyclic frameworks through intramolecular cyclization and heteroatom incorporation [13–17]. Building on these studies, we subsequently introduced 1,2-dicarboxy-functionalized Cp ligands as complementary precursors for the construction of carbocyclic and heterocyclic fused systems. In this context, we previously reported the synthesis and structural characterization of pentamethylruthenocene-1,2-dicarboxylic acid and its fused anhydride as precursors in the preparation of metallocene-fused quinone systems [18]. These studies collectively demonstrate that structurally analogous Cp-fused frameworks can be supported by both manganese tricarbonyl and ruthenocene fragments and provide a foundation for further extension to other heterocycle-fused systems.

Despite significant advances in cyclopentadienyl ligand functionalization, heterocycle-fused Cp systems remain relatively unexplored, especially in understanding how different metal fragments influence the properties of a common fused ligand framework. In particular, the electronically distinct $Mn(CO)_3$ and Ru(Cp*) fragments provide an opportunity to examine how the metal center affects bonding and electron distribution within related fused Cp systems. Motivated by our previous work on fused anhydride systems [18], we sought to extend this chemistry to related heterocycles incorporating sulfur and nitrogen. Herein, we report the synthesis, spectroscopic characterization, and comparative structural analysis of 5,5-fused thioanhydride and imide derivatives of cyclopentadienylmanganese tricarbonyl and pentamethylruthenocene.

2. Experimental

2.1. General Considerations

All reactions were carried out under a nitrogen atmosphere using standard Schlenk techniques unless otherwise noted. Solvents were dried and distilled under nitrogen using standard methods. Commercial reagents were used as received unless otherwise specified. ^1H and ^{13}C NMR spectra were recorded at ca. 22 °C on a Varian Gemini-400 spectrometer (Varian, Inc., Palo Alto, CA, USA) and referenced to residual solvent resonances. Infrared spectra were recorded using FTIR (ATI Mattson Instruments, Inc., Madison, WI, USA) or ATR (Bruker Scientific LLC, Billerica, MA, USA) spectrometers. Mass spectra were obtained at the University of Kentucky Mass Spectrometry Facility. Electron ionization (EI) mass spectra were recorded at 70 eV on a Thermo Finnigan PolarisQ quadrupole ion trap mass spectrometer (Thermo Finnigan, San Jose, CA, USA) using a heatable direct-insertion probe. Melting points were determined using a Thomas–Hoover capillary melting point apparatus and are uncorrected. The complexes $[MnBr(CO)_5]$ [19], $[Ru(\mu_3\text{-}Cl)Cp^*]_4$ [20], $[Mn(CO)_3\{\eta^5\text{-}C_5H_3(CO_2Ph)_2\text{-}1,2\}$ (**1a**) [9], together with the previously reported ruthenium complexes $[Ru\{\eta^5\text{-}C_5H_3(CO_2Ph)_2\text{-}1,2\}(Cp^*)]$ (**1b**), $[Ru\{\eta^5\text{-}C_5H_3(CO_2H)_2\text{-}1,2\}(Cp^*)]$ (**2b**), and $[Ru\{\eta^5\text{-}C_5H_3(CO)_2O\text{-}1,2\}(Cp^*)]$ (**5b**) [18], were prepared according to literature procedures.

2.2. X-Ray Crystallography

Single-crystal X-ray diffraction data for compounds **2a**, **3a**, and **6a** were collected at 90.0(2) K on a Nonius KappaCCD diffractometer using Mo Kα radiation, while data for **4a** and **4b** were collected at 90.0(2) K on a Bruker–Nonius X8 Proteum diffractometer (Bruker AXS LLC, Madison, WI) using graded multilayer-focused Cu Kα radiation. Raw data were integrated, scaled, merged, and corrected for Lorentz–polarization effects using the HKL-SMN package [21] for data collected on the KappaCCD instrument and APEX2 [22] for data collected on the X8 Proteum system. Absorption corrections were applied using SCALEPACK [21], SADABS [23], or XABS2 [24] as appropriate. The structures were solved by direct methods using SHELXS-97 [25] and refined against F^2 by full-matrix least-squares methods using SHELXL [26]. Non-hydrogen atoms were refined anisotropically, and hydrogen atoms were located in difference Fourier maps and subsequently placed in calculated positions and refined using riding models. Atomic scattering factors were taken from the International Tables for Crystallography [27]. Thermal ellipsoid plots were generated using the program PrimeXP [28], whereas molecular interaction diagrams shown in Supporting Information were prepared using Mercury [29].

2.3. Synthesis and Characterization

[Mn(CO)$_3${η^5-C$_5$H$_3$(CO$_2$H)$_2$-1,2}] (2a)

Diester **1a** (200 mg, 0.450 mmol) was dissolved in CH_2Cl_2 (6 mL) and MeOH (0.6 mL) in a 125 mL Schlenk flask under nitrogen. A solution of NaOH in MeOH (2 M, 1.2 mL, 2.4 mmol) was added dropwise, and the reaction mixture was stirred at room temperature for 4 h, during which a pale-yellow precipitate formed. The precipitate was dissolved in water (20 mL) and the solution was extracted with CH_2Cl_2 (2 × 10 mL) to remove unreacted starting material and other organic-soluble impurities. The aqueous layer was collected, acidified to pH ≈ 2 with concentrated HCl, and extracted with Et_2O (2 × 10 mL). The combined organic extracts were dried ($MgSO_4$), filtered, and concentrated under reduced pressure. The residue was washed with hexane (3 × 10 mL) and dried under vacuum to afford **2a** (118 mg, 90%) as a dark yellow solid. Single crystals suitable for X-ray diffraction were obtained by vapor diffusion of hexane into a concentrated CH_2Cl_2 solution of the product. Mp: 162–164 °C. ^{1}H NMR (400 MHz, DMSO-d$_6$): δ 5.08 (t, 1H, Cp-H), 5.61 (d, 2H, Cp-H), 5.0–5.5 (br, CO_2H). ^{13}C{^{1}H} NMR (100 MHz, acetone-d$_6$): δ 84.0, 94.8, 112.2 (Cp), 164.4 (CO_2H), 223.0 (Mn–CO). IR (KBr): ν = 3453 (O–H), 2038, 2040, 1958 (Mn–CO), 1706 cm^{-1} (C=O). MS (EI) m/z: 292 (M^+), 208 (M^+–3CO). The molecular structure of **2a** was confirmed by single-crystal X-ray diffraction.

[Mn(CO)$_3${η^5-C$_5$H$_3$(COCl)$_2$-1,2}] (3a)

Oxalyl chloride (0.50 mL, 6.5 mmol) and DMF (1 drop) were added to a stirred suspension of **2a** (100 mg, 0.34 mmol) in benzene (15 mL). The reaction mixture was stirred at room temperature for 4 h. Volatiles were removed under reduced pressure, and the residue was extracted with dry hexane under nitrogen. Removal of solvent afforded **3a** (73 mg, 65%) as an orange-yellow powder. Single crystals suitable for X-ray diffraction were obtained by cooling a saturated hexane solution at −10 °C for 3 days. Mp: 61–62 °C. ^{1}H NMR (400 MHz, acetone-d$_6$): δ 5.41 (t, 1H, J = 2.9 Hz, Cp–H), 6.34 (d, 2H, J = 2.9 Hz, Cp–H). ^{13}C{^{1}H} NMR (100 MHz, acetone-d$_6$): δ 82.8, 91.9, 98.2 (Cp), 162.2 (COCl), 221.4 (Mn–CO). IR (Nujol): ν 2049, 1984 (Mn–CO), 1796 cm^{-1} (acyl chloride C=O). MS (EI): m/z 328 (M^+), 330 (M^+ + 2), 293 (M^+ − Cl). The molecular structure of **3a** was confirmed by single-crystal X-ray diffraction.

[Mn(CO)$_3${η^5-C$_5$H$_3$(CO)$_2$S-1,2}] (4a)

Oxalyl chloride (0.50 mL, 6.5 mmol) and DMF (10 μL) were added to a stirred suspension of **2a** (100 mg, 0.34 mmol) in benzene (15 mL) under nitrogen, and the mixture was

stirred at room temperature for 4 h. Volatiles were removed under reduced pressure. The residue was treated with dry KF (80 mg, 1.38 mmol), 18-crown-6 (10 mg), and anhydrous CH_2Cl_2 (20 mL), followed by addition of hexamethyldisilathiane (243 mg, 1.36 mmol). After stirring at room temperature for 6 h, the mixture was filtered through a thin pad of silica, concentrated in vacuo, and the residue was triturated with cold pentane to afford **4a** (66 mg, 66% from **2a**) as a light orange solid. Single crystals suitable for X-ray diffraction were obtained from a saturated CH_2Cl_2 solution by partial evaporation under a slow stream of hexane-saturated nitrogen. Mp: 99–101 °C. ^{1}H NMR (400 MHz, acetone-d_6): δ 5.59 (t, J = 2.8 Hz, 1H, Cp–H), 5.91 (d, J = 2.9 Hz, 2H, Cp–H). ^{13}C{^{1}H} NMR (100 MHz, acetone-d_6): δ 83.8, 91.4, 100.3 (Cp), 186.1 (C=O), 222.4 (Mn–CO). IR (ATR): ν 2035, 1950 (Mn–CO), 1720, 1689 cm^{-1} (C=O). MS (EI): m/z 290 (M^+). The molecular structure of **4a** was confirmed by single-crystal X-ray diffraction.

[Ru{η^5-C$_5$H$_3$(CO)$_2$S-1,2}(Cp*)] (4b)

Oxalyl chloride (88 µL, 1.04 mmol) and DMF (10 µL) were added to a stirred suspension of **2b** (100 mg, 0.26 mmol) in benzene (20 mL) under a nitrogen atmosphere, and the mixture was stirred at room temperature for 3 h. Volatiles were removed under reduced pressure. The residue was treated with dry KF (148 mg, 2.56 mmol), 18-crown-6 (20 mg), and anhydrous CH_2Cl_2 (20 mL), followed by addition of hexamethyldisilathiane (0.27 mL, 1.28 mmol). After stirring at room temperature for 10 h, volatiles were removed in vacuo and the crude product was purified by silica gel chromatography (EtOAc/hexane, 1:5) to afford **4b** (75 mg, 75%) as a light yellow crystalline solid. Single crystals suitable for X-ray diffraction were obtained from a saturated CH_2Cl_2 solution by partial evaporation under a slow stream of hexane-saturated nitrogen. Mp: 252–254 °C. ^{1}H NMR (400 MHz, $CDCl_3$): δ 1.76 (s, 15H, Cp*), 4.85 (t, J = 2.6 Hz, 1H, Cp–H), 4.93 (d, J = 2.6 Hz, 2H, Cp–H). ^{13}C{^{1}H} NMR (100 MHz, $CDCl_3$): δ 10.2 (Cp*–CH_3), 72.0 (Cp*), 84.0, 88.3, 89.5 (Cp), 187.3 (C=O). IR (ATR): ν 1708, 1679 cm^{-1} (C=O), 1277 cm^{-1} (C–S). MS (EI): m/z 388 (M^+).

[Mn(CO)$_3${η^5-C$_5$H$_3$(CO)$_2$O-1,2}] (5a)

Trifluoroacetic anhydride (10 mL) was added to a suspension of **2a** (200 mg, 0.68 mmol) in a 100 mL Schlenk flask under nitrogen, and the reaction mixture was heated at reflux for 3 h. After cooling to room temperature, volatiles were removed under reduced pressure. The residue was dissolved in benzene (15 mL), filtered via cannula, and concentrated to dryness to afford **5a** (87 mg, 46%) as a deep yellow, moisture-sensitive solid. ^{1}H NMR (400 MHz, acetone-d_6): δ 5.57 (t, 1H, J = 2.4 Hz, Cp–H), 5.90 (d, 2H, J = 2.4 Hz, Cp–H). ^{13}C{^{1}H} NMR (100 MHz, acetone-d_6): δ 92.0, 92.6, 93.1 (Cp carbons), 161.0 (anhydride C=O), 222.1 (Mn–CO). IR (ATR): ν 2039, 1944 (Mn–CO), 1788, 1739 cm^{-1} (anhydride C=O). MS (EI): m/z 273 (M^+).

[Mn(CO)$_3${η^5-C$_5$H$_3$(CO)$_2$N-4-C$_6$H$_4$CH$_3$-1,2}] (6a)

Trifluoroacetic anhydride (5 mL) was added to **2a** (100 mg, 0.34 mmol) in a 100 mL Schlenk flask under nitrogen, and the mixture was refluxed for 3 h. After cooling to room temperature, volatiles were removed under reduced pressure. The residue was dissolved in benzene (15 mL), and *p*-toluidine (37 mg, 0.34 mmol) was added. The reaction mixture was stirred at room temperature for 10 h, followed by the addition of oxalyl chloride (0.12 mL, 1.36 mmol) and DMF (10 µL). The mixture was heated at reflux for 2 h, cooled, and concentrated in vacuo. The crude product was purified by silica gel column chromatography (Et_2O/hexane, 1:1), and the product-containing fraction was concentrated and triturated with cold pentane to afford **6a** (52 mg, 42% from **2a**) as a light yellow solid. Analytically pure material was obtained by recrystallization from CH_2Cl_2/hexane. Single crystals suitable for X-ray diffraction were obtained from a saturated CH_2Cl_2 solution by partial evaporation under a slow stream of hexane-saturated nitrogen. Mp: 198–200 °C. ^{1}H NMR (400 MHz, acetone-d_6): δ 2.37 (s, 3H, CH_3), 5.38 (t, 1H, J = 2.8 Hz, Cp–H), 5.86

(d, 2H, *J* = 2.8 Hz, Cp–H), 7.19 (d, 2H, *J* = 8.0 Hz, Ar), 7.31 (d, 2H, *J* = 8.0 Hz, Ar). $^{13}C\{^1H\}$ NMR (100 MHz, acetone-d_6): δ 21.7 (CH_3), 83.5, 88.0, 92.5 (Cp), 120.5, 128.1, 130.4, 139.2 (Ar), 165.1 (imide C=O), 224.7 (Mn–CO). IR (ATR): ν 2046, 2028 (Mn–CO), 1725, 1714 cm^{-1} (imide C=O). MS (EI): m/z 363 (M^+). The molecular structure of **6a** was confirmed by single-crystal X-ray diffraction.

[Ru{η^5-$C_5H_3(CO)_2$N-4-$C_6H_4CH_3$-1,2}(Cp*)] (6b)

p-Toluidine (13 mg, 0.12 mmol) was added to a stirred solution of **5b** (43 mg, 0.12 mmol) in THF (20 mL) under nitrogen, and the mixture was refluxed overnight until complete consumption of the starting material. After cooling to room temperature, oxalyl chloride (20 µL, 0.24 mmol) and DMF (5 µL) were added, and the reaction mixture was refluxed for 5 h. The mixture was cooled and concentrated under reduced pressure. The crude product was purified by silica gel column chromatography (EtOAc/hexane, 1:5), and the product-containing fraction was concentrated and triturated with cold pentane to afford **6b** (13 mg, 31%) as a pale yellow solid. ^1H NMR (400 MHz, $CDCl_3$): δ 1.82 (s, 15H, Cp*), 2.34 (s, 3H, CH_3), 4.68 (t, 1H, *J* = 2.4 Hz, Cp–H), 4.92 (d, 2H, *J* = 2.4 Hz, Cp–H), 7.50 (AA′BB′, 2H, Ar), 7.68 (AA′BB′, 2H, Ar). $^{13}C\{^1H\}$ NMR (100 MHz, $CDCl_3$): δ 11.2 ($CpCH_3$), 23.9 (CH_3), 68.4 (CpC), 70.7, 80.8, 88.9 (Cp), 126.6, 129.0, 131.1, 132.6 (Ar), 167.9 (imide C=O). IR (KBr): ν 1654, 1629 cm^{-1} (imide C=O). MS (EI): m/z 461 (M^+).

3. Results and Discussion

3.1. Synthesis and Characterization of Cp-Fused Thioanhydrides and Imides

The synthetic routes to the Cp-fused heterocyclic complexes are outlined in Scheme 1. Diesters **1a** [9] and **1b** [18] were hydrolyzed to the corresponding 1,2-dicarboxylic acids **2a** and **2b**. While the ruthenocene derivative **2b** has been reported previously [18], attempts to hydrolyze the cymantrene diester **1a** using aqueous NaOH were unsuccessful. Consequently, saponification of **1a** was performed using non-aqueous conditions, employing NaOH in a mixed solvent system of $MeOH/CH_2Cl_2$ [30] to afford the manganese dicarboxylic acid **2a** in 90% yield. Formation of the diacid is supported by the disappearance of the resonances corresponding to phenyl substituents in the ^1H NMR and the appearance of a strong C=O stretching band at 1706 cm^{-1}. The $Mn(CO)_3$ fragment remains intact, as evidenced by characteristic carbonyl absorptions from 2038–1958 cm^{-1}.

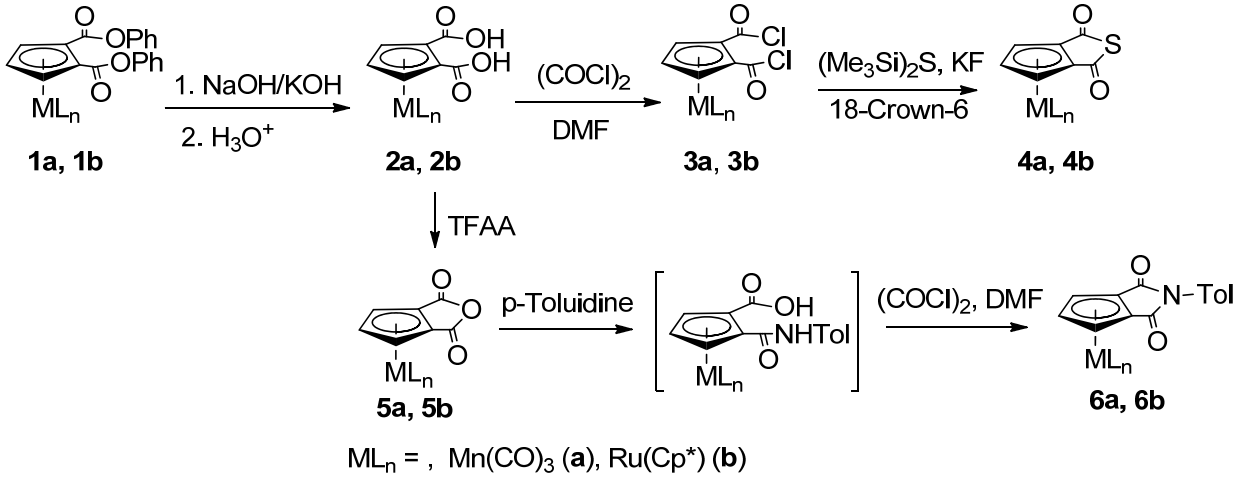

Scheme 1. Synthetic routes to 5,5-fused heterocyclic derivatives of cyclopentadienylmanganese tricarbonyl and pentamethylruthenocene complexes.

Treatment of **2a** and **2b** with oxalyl chloride in the presence of catalytic DMF afforded the corresponding diacyl chlorides **3a** and **3b**. While the synthesis and characterization of pentamethylruthenocene-1,2-diacyl chloride **3b** have been reported previously [18], the

cymantrene analogue, **3a** was isolated and fully characterized in this work. Formation of the acyl chloride is evidenced by strong IR carbonyl absorption at 1796 cm^{-1}. The manganese diacyl chloride **3a** exhibited lower stability toward ambient conditions than the corresponding ruthenium derivative **3b**, undergoing gradual decomposition (tarnishing) during storage.

Although **3a** and **3b** were isolated and characterized, cyclization to **4a** (67%) and **4b** (75%) was carried out using in situ-generated diacyl chlorides. Following a procedure reported by Ando et al. [31], treatment of the in situ-generated diacyl chlorides with hexamethyldisilathiane in the presence of KF and 18-crown-6 afforded the corresponding Cp-fused thioanhydrides. Formation of the thioanhydride ring is supported by characteristic splitting of the carbonyl absorptions in the IR spectra (1689 and 1720 cm^{-1} for **4a**; 1679 and 1708 cm^{-1} for **4b**).

Dehydration of the dicarboxylic acid **2a** with trifluoroacetic anhydride afforded the fused anhydride **5a** in 46% yield. In contrast to the previously reported ruthenocene analogue **5b** [18], the manganese derivative **5a** was found to be significantly more sensitive to ambient conditions, undergoing gradual decomposition upon exposure to air within 24 h and therefore requiring generation in situ for subsequent transformations.

The reactivity of the fused anhydrides toward amines was examined using *p*-toluidine. Treatment of **5a** and **5b** with *p*-toluidine resulted in ring opening to give the corresponding amide–carboxylic acids (see Scheme 1). Direct conversion of these intermediates to the imide was not observed. Instead, treatment with oxalyl chloride in the presence of catalytic DMF promoted cyclization to produce the fused imide complexes **6a** (42%) and **6b** (31%). The lower yield of **6b** is consistent with the reduced electrophilicity of the carbonyl groups caused by the presence of the electron-rich Ru(Cp*) fragment. The formation of the imide functionality is supported by characteristic carbonyl absorptions in the IR spectra (1725 and 1714 cm^{-1} for **6a**; 1654 and 1629 cm^{-1} for **6b**).

Spectroscopic data for complexes **2**–**6** are summarized in Table 1. Comparison of analogous $Mn(CO)_3$ and Ru(Cp*) derivatives reveals consistent metal-dependent electronic trends. Relative to the electron-rich Ru(Cp*) fragment, the $Mn(CO)_3$ unit, which contains strongly π-accepting carbonyl ligands, withdraws electron density from the cyclopentadienyl framework. As a result, the manganese complexes generally exhibit downfield Cp proton resonances in the NMR spectra and higher carbonyl stretching frequencies in the IR spectra than their ruthenocene counterparts. These trends are consistent with reduced electron density within the fused ligand framework, leading to stronger carbonyl bonding and correspondingly higher ν(C=O) values in the manganese series.

Table 1. Selected ^1H NMR, ^{13}C NMR, and IR spectroscopic data for complexes **2**–**6**.

Compd	Metal Fragment	δ_H (CpH, t) ppm	δ_H (CpH, d) ppm	δ_C (C=O) ppm	ν (C=O) cm^{-1}
2a	$Mn(CO)_3$	5.08	5.61	164.4	1706
2b †	Ru(Cp*)	4.81	5.07	169.9	1603
3a	$Mn(CO)_3$	5.41	6.34	162.2	1796
3b †	Ru(Cp*)	5.12	5.43	162.7	1801
4a	$Mn(CO)_3$	5.59	5.91	186.1	1689, 1720
4b	Ru(Cp*)	4.85	4.93	187.3	1679, 1708
5a	$Mn(CO)_3$	5.57	5.90	161.0	1739, 1788
5b †	Ru(Cp*)	5.03	5.12	163.8	1765, 1820
6a	$Mn(CO)_3$	5.38	5.86	165.1	1714, 1725
6b	Ru(Cp*)	4.68	4.92	167.9	1629, 1654

† Data from ref. [18].

3.2. Molecular Structures

Single crystals suitable for X-ray diffraction were obtained for compounds **2a**, **3a**, **4a**, **4b**, and **6a**, and their molecular structures are shown in Figures 1–3. Selected crystallographic parameters are summarized in Table 2, while comparative structural parameters are collected in Table S1 (see Supplementary Materials).

Structures **2a** and **4a** each crystallized with two crystallographically independent molecules in the asymmetric unit ($Z' = 2$), whereas **3a**, **4b**, and **6a** contain a single molecule in the asymmetric unit ($Z' = 1$). The independent molecules in **2a** and **4a** exhibit very similar metrical parameters and differ only slightly in the orientations of the substituents relative to the cyclopentadienyl framework (Table S2). The molecular structure of **2a** confirms the formation of the cymantrene-1,2-dicarboxylic acid framework. Two crystallographically independent molecules are present in the asymmetric unit. In both molecules, the carboxylic acid groups adopt nearly coplanar orientations relative to the cyclopentadienyl ring, aided by intramolecular O–H···O hydrogen bonding. In the solid state, the molecules further assemble through intermolecular O–H···O hydrogen-bonding interactions to form hydrogen-bonded chains (Figure S1 and Table S2). The carboxylic acid substituents deviate only slightly from the Cp plane, with interplanar angles of 2.6–9.0° (Table S2). The Mn–Cp centroid distances of 1.766–1.769 Å are consistent with typical η^5-coordinated cymantrene complexes and are comparable to those reported for related cyclopentadienylmanganese tricarbonyl derivatives [9,15].

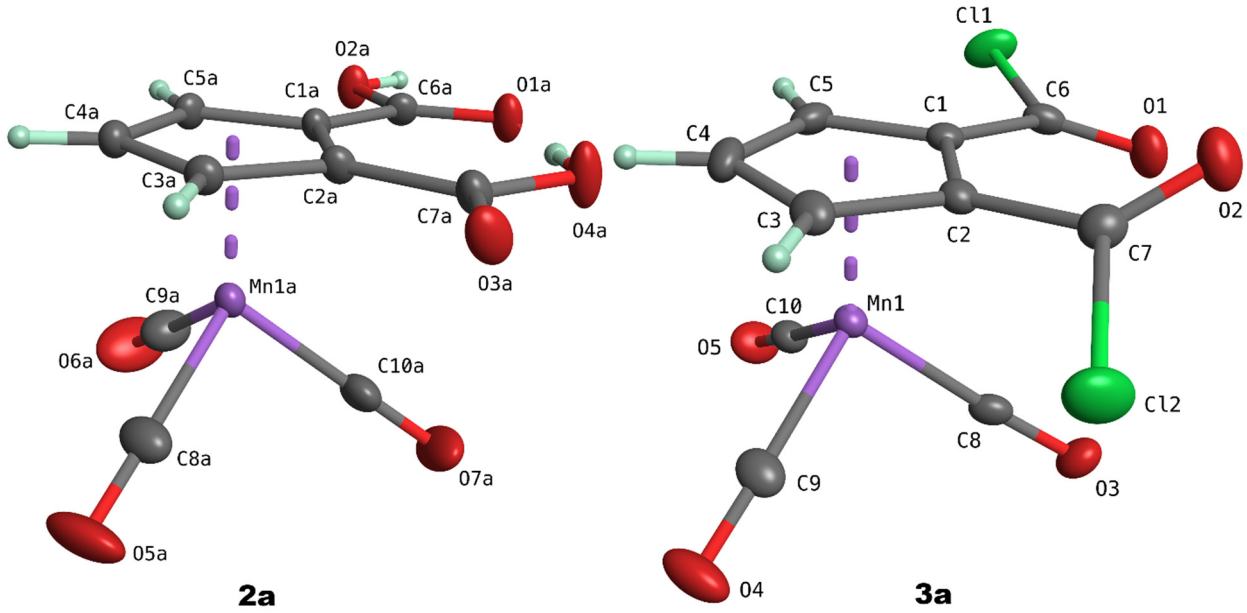

Figure 1. Thermal ellipsoid plots (50% probability) of **2a** and **3a**. For **2a**, only one of the two crystallographically independent molecules is shown for clarity. Selected bond lengths (Å) for **2a**: Mn1a–C1a 2.1201(17), Mn1a–C2a 2.1282(18), Mn1a–C3a 2.1490(19), Mn1a–C4a 2.1715(18), Mn1a–C5a 2.1514(18), Mn1a–C8a 1.805(2), Mn1a–C9a 1.809(2), Mn1a–C10a 1.811(2), O1a–C6a 1.230(2), O3a–C7a 1.224(2). Selected bond lengths (Å) for **3a**: Mn1–C1 2.1220(13), Mn1–C2 2.1121(13), Mn1–C3 2.1444(14), Mn1–C4 2.1715(15), Mn1–C5 2.1507(14), Mn1–C8 1.8116(15), Mn1–C9 1.8085(16), Mn1–C10 1.8104(15), C6–O1 1.1809(18), C7–O2 1.1877(18); C6–Cl1 1.7864(14), C7–Cl2 1.7792(15).

Conversion of **2a** to the diacyl chloride **3a** results in noticeable geometric changes within the ligand framework. The acyl chloride substituents exhibit significantly larger deviations from the Cp plane (10.7–29.5°) relative to the carboxylic acid groups in **2a** (Table S2). Correspondingly, the substituent carbonyl bond lengths shorten from 1.222–1.230 Å in **2a** to 1.181–1.188 Å in **3a**. Despite these changes, the Mn–Cp centroid distance remains essen-

tially unchanged at 1.764 Å, indicating minimal perturbation of the η^5-cyclopentadienyl coordination upon conversion of the carboxylic acid groups to acyl chlorides.

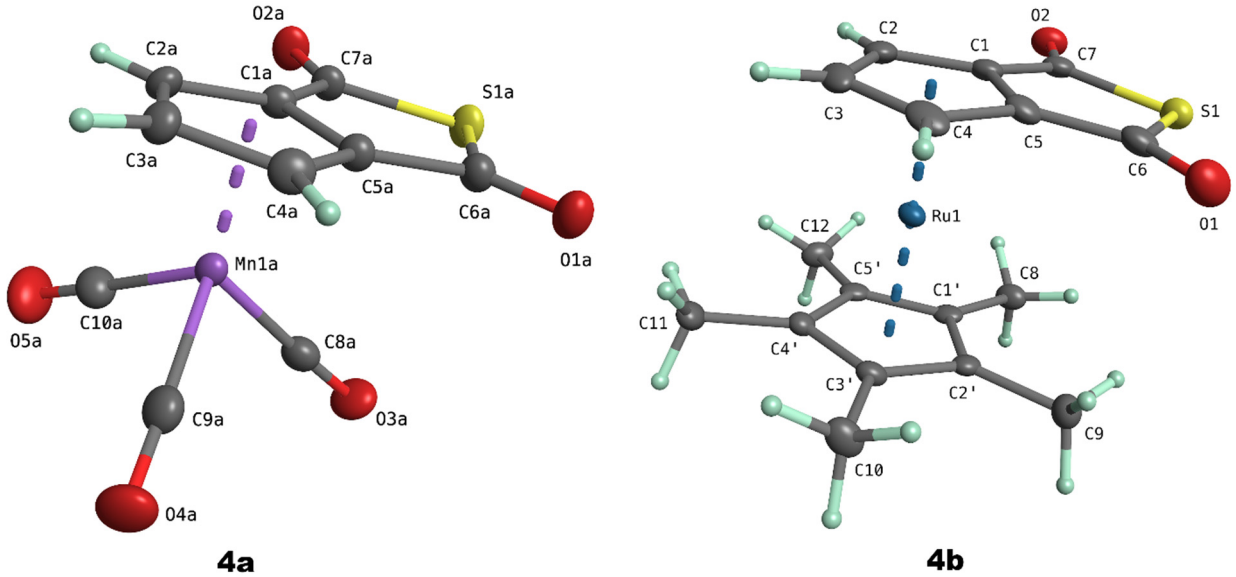

Figure 2. Thermal ellipsoid plots (50% probability) of **4a** and **4b**. For **4a**, only one of the crystallographically independent molecules is shown for clarity. Selected bond lengths (Å) and angles (°) for **4a**: Mn1a–C1a 2.124(2), Mn1a–C2a 2.154(2), Mn1a–C3a 2.159(2), Mn1a–C4a 2.155(2), Mn1a–C5a 2.116(2), Mn1a–C8a 1.811(3), Mn1a–C9a 1.807(3), Mn1a–C10a 1.805(3), C6a-O1a 1.197(3), C7a-O2a 1.199(3), C6a–S1a 1.814(3), C7a-S1A 1.823(3); C6a-S1a-C7a 94.13(11). Selected bond lengths (Å) and angles (°) for **4b**: Ru1–C1 2.174(2), Ru1–C2 2.198(2), Ru1–C3 2.196(2), Ru1–C4 2.187(3), Ru1–C5 2.168(2); C6-O1 1.204(3), C7-O2 1.206(3), C6-S1 1.821(3), C7-S1 1.829(3); C6–S1–C7 94.01(12).

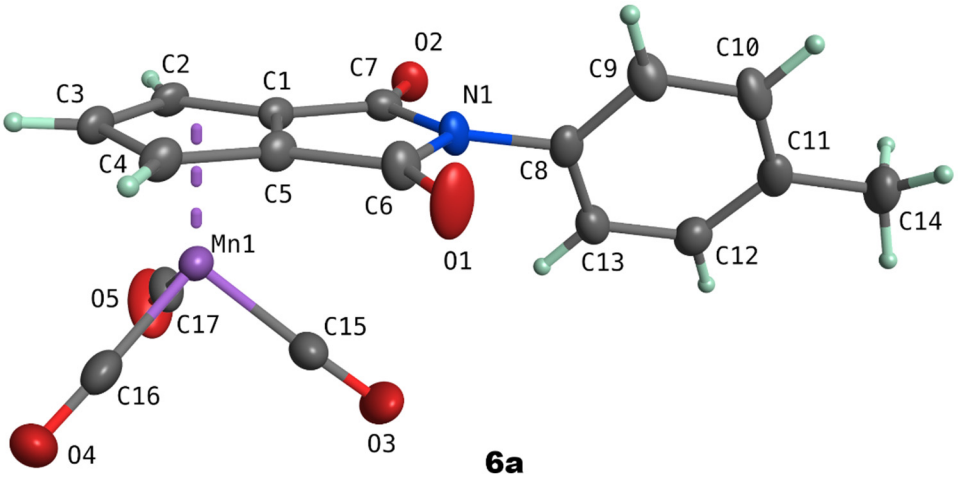

Figure 3. Thermal ellipsoid plot (50% probability) of **6a**. Selected bond lengths (Å) and angles (°): Mn1–C1 2.127(3), Mn1–C2 2.147(2), Mn1–C3 2.148(3), Mn1–C4 2.154(3), Mn1–C5 2.114(2), Mn1-C15 1.795(3), Mn1-C16 1.798(3), Mn1-C17 1.795(4), C6-O1 1.203(3), C7-O2 1.210(3), C6-N1 1.412(3), C7–N1 1.420(3), C8-N1 1.437(3) C6–N1–C7 113.4(2).

The molecular structures of the fused thioanhydrides **4a** and **4b** confirm successful annulation of the heterocyclic framework onto the cyclopentadienyl ligand. In **4a**, two crystallographically independent molecules are present, both exhibiting nearly coplanar fused thioanhydride rings relative to the Cp framework, with interplanar angles of approximately 1.3° (Table S2). Similarly, the ruthenocene derivative **4b** retains an essentially planar fused framework, with a Cp/thioanhydride interplanar angle of 4.2°. The Ru–Cp and Ru–Cp*

centroid distances of 1.814 and 1.803 Å, respectively, are comparable to those reported for pentamethylruthenocene-fused cyclic anhydride [18]. Likewise, the Mn–Cp centroid distances in **4a** (1.769–1.770 Å) remain consistent with those observed for related 5,5-fused cyclopentadienylmanganese tricarbonyl derivatives [15]. Weak intermolecular interactions are also observed in crystal packing. In **4a**, neighboring molecules are associated through weak O···π contacts involving a thioanhydride carbonyl oxygen atom and a neighboring Cp ring centroid (Figure S2). In **4b**, weak π-associated intermolecular contacts are present, including a Cp* C–H···π interaction and a slipped Cp···Cp* contact (Figure S3).

Table 2. Crystal data and structure refinement parameters for complexes **2a**, **3a**, **4a**, **4b**, and **6a**.

Parameter	2a	3a	4a	4b	6a
CCDC number	2541846	2541843	2541845	2541844	2541847
Empirical formula	$C_{10}H_5MnO_7$	$C_{10}H_3Cl_2MnO_5$	$C_{10}H_3MnO_5S$	$C_{17}H_{18}O_2RuS$	$C_{17}H_{10}MnNO_5$
Formula weight	292.08	328.96	290.12	387.44	363.20
Temperature (K)	90.0(2)	90.0(2)	90.0(2)	90.0(2)	90.0(2)
Wavelength (Å)	0.71073	0.71073	1.54178	1.54178	0.71073
Crystal system	Monoclinic	Triclinic	Monoclinic	Monoclinic	Orthorhombic
Space group	$P2_1/c$	P-1	I2/a	$P2_1/c$	Pbca
a (Å)	7.5419(1)	6.9962(1)	23.6290(8)	7.2286(2)	15.5245(3)
b (Å)	11.7432(1)	7.2154(1)	7.7330(2)	15.6173(4)	15.4893(3)
c (Å)	24.5013(3)	12.8685(3)	24.3404(7)	14.5631(3)	12.7932(3)
α (°)	90	88.6306(9)	90	90	90
β (°)	92.1283(4)	87.9181(9)	111.390(1)	111.750(1)	90
γ (°)	90	67.0535(9)	90	90	90
Volume (Å^3)	2168.49(4)	597.775(19)	4141.2(2)	1527.01(7)	3076.30(11)
Z, Z′	8, 2	2, 1	16, 2	4, 1	8, 1
ρcalc (g cm^{-3})	1.789	1.828	1.861	1.685	1.568
μ (mm^{-1})	1.242	1.558	12.360	9.592	0.885
F(000)	1168	324	2304	784	1472
Reflections collected	44633	5417	39499	24083	6636
Independent reflections	4959	2733	3761	2797	3523
Goodness-of-fit on F^2	1.095	1.074	1.029	1.081	1.016
Final R indices [I > 2σ(I)]	R_1 = 0.0289, wR_2 = 0.0685	R_1 = 0.0223, wR_2 = 0.0521	R_1 = 0.0306, wR_2 = 0.0774	R_1 = 0.0229, wR_2 = 0.0620	R_1 = 0.0428, wR_2 = 0.1022
wR_2 (all data)	0.0734	0.0534	0.0821	0.0633	0.1214

The molecular structure of **6a** confirms formation of the Cp-fused imide framework. The imide ring remains essentially coplanar with the cyclopentadienyl ligand, exhibiting a Cp/imide interplanar angle of 1.6° (Table S2), consistent with efficient conjugation across the fused framework. The imide carbonyl bond lengths [1.203(3) and 1.210(3) Å] and C–N bond distances [1.412(3) and 1.420(3) Å] are consistent with significant delocalization within the imide unit. In contrast, the *p*-tolyl substituent is rotated substantially out of the imide plane, with an interplanar angle of 70.43°, thereby reducing conjugation between the aryl substituent and the imide nitrogen. The widened C–N–C angle of 113.4(2)° further supports partial sp^2 hybridization and delocalization at nitrogen. In the solid state, the crystal packing of **6a** features a directional intermolecular C–H···π interaction between a cyclopentadienyl proton and the neighboring *p*-tolyl ring (Figure S4).

Overall, the crystallographic data demonstrate that annulation preserves the metallocene coordination geometry while enforcing near coplanarity of the fused heterocyclic frameworks with the cyclopentadienyl ligand.

4. Conclusions

A series of 5,5-fused heterocyclic derivatives of cyclopentadienylmanganese tricarbonyl and pentamethylruthenocene has been synthesized from 1,2-dicarboxylate precursors

and characterized by spectroscopic methods, with representative compounds further confirmed by single-crystal X-ray diffraction. The results demonstrate that thioanhydride, anhydride, and imide functionalities can be efficiently incorporated into cyclopentadienyl frameworks without significant perturbation of the metal–cyclopentadienyl coordination geometry, as evidenced by minimal variation in Mn–C and Ru–C bond metrics across the series. Crystallographic analyses further reveal that annulation enforces near coplanarity of the fused heterocyclic frameworks with the cyclopentadienyl ligand, thereby promoting conjugation within the fused systems.

In contrast, systematic differences in spectroscopic properties highlight the dominant role of the metal fragment in modulating the electronic characteristics of the fused ligand framework. Relative to the electron-rich Ru(Cp*) derivatives, the electron-deficient $Mn(CO)_3$ complexes exhibit consistently higher ν(C=O) stretching frequencies and downfield NMR resonances, reflecting reduced electron density within the ligand system. The crystal packing analyses additionally reveal diverse intermolecular interactions, including O–H···O hydrogen bonding, O···π contacts, and C–H···π interactions, depending on the heterocyclic functionality present. Collectively, these results establish fused cyclopentadienyl heterocycles as structurally robust and electronically tunable organometallic platforms for investigating metal–ligand electronic communication and designing extended conjugated organometallic architectures.

Supplementary Materials: The following supporting information can be downloaded at: https://www.mdpi.com/article/10.3390/cryst16070409/s1, Crystallographic data for compounds **2a**, **3a**, **4a**, **4b**, and **6a** have been deposited with the Cambridge Crystallographic Data Centre under deposition numbers 2541843–2541848. These data can be obtained free of charge from www.ccdc.cam.ac.uk/data_request/cif (accessed on 21 May 2026).

Author Contributions: Conceptualization, U.R.P. and J.P.S.; Methodology, U.R.P. and J.P.S.; Software, S.P.; Validation, U.R.P. and J.P.S.; Formal analysis, U.R.P. and J.P.S.; Investigation, U.R.P.; Resources, J.P.S.; Data curation, U.R.P. and S.P.; Writing—original draft, U.R.P.; Writing—review & editing, U.R.P., S.P. and J.P.S.; Visualization, U.R.P. and S.P.; Supervision, J.P.S.; Project administration, J.P.S.; Funding acquisition, J.P.S. All authors have read and agreed to the published version of the manuscript.

Funding: This research received no external funding.

Data Availability Statement: The original contributions presented in this study are included in the article/Supplementary Materials. Further inquiries can be directed to the corresponding author.

Acknowledgments: The authors extend their appreciation to the Department of Chemistry, University of Kentucky, for providing funds for purchasing chemicals and characterization of the compounds. During the preparation of this manuscript, the first author used OpenAI (ChatGPT Plus) for the purposes of language editing and writing assistance to improve readability. The authors have reviewed and edited the output and take full responsibility for the content of this publication.

Conflicts of Interest: The authors declare no conflicts of interest.

References

1. Halterman, R.L. Synthesis and applications of chiral cyclopentadienylmetal complexes. *Chem. Rev.* **1992**, *92*, 965–994. [CrossRef]
2. Shapiro, P.J. The evolution of the ansa-bridge and its effect on the scope of metallocene chemistry. *Coord. Chem. Rev.* **2002**, *231*, 67–81. [CrossRef]
3. Crabtree, R.H. *The Organometallic Chemistry of the Transition Metals*, 7th ed.; John Wiley & Sons: Hoboken, NJ, USA, 2019; pp. 159–189.
4. Astruc, D. Why is ferrocene so exceptional? *Eur. J. Inorg. Chem.* **2017**, *2017*, 6–29.
5. VanderWeide, A.; Prokopchuk, D.E. Cyclopentadienyl ring activation in organometallic chemistry and catalysis. *Nat. Rev. Chem.* **2023**, *7*, 561–572. [CrossRef] [PubMed]
6. Erb, W.; Mongin, F. Twofold ferrocene C–H lithiations for one-step difunctionalizations. *Synthesis* **2019**, *51*, 146–160.

7. Vollgraff, T.; Sundermeyer, J. Highly Selective Ortho-Directed Dicarboxylation of Cyclopentadiene by Methylcarbonates and CO_2 or COS–First Insight into Co-ordination Chemistry of New Ambident Ligands. *Chem. Eur. J.* **2021**, *27*, 8517–8527. [PubMed]
8. Ursillo, S.; Can, D.; N'Dongo, H.W.P.; Schmutz, P.; Spingler, B.; Alberto, R. Cyclopentadienyl Chemistry in Water: Synthesis and Properties of Bifunctionalized $[(\eta^5\text{-}C_5H_3\{COOR\}_2)M(CO)_3]$ (M = Re and ^{99}mTc) Complexes. *Organometallics* **2014**, *33*, 6945–6952.
9. Busetto, L.; Cassani, M.C.; Zanotti, V.; Albano, V.G.; Sabatino, P. Coordination Chemistry of Cyclopentadienyl Ester-Disubstituted Ligands. Synthesis and Solid State Structures of $[Na([18]\text{-crown-}6)][C_5H_3(CO_2Et)_2\text{-}1,2]$ and $[Mn\{C_5H_3(CO_2Ph)_2\text{-}1,2\}(CO)_3]$. *Organometallics* **2001**, *20*, 282–288.
10. Valderas, C.; Casarrubios, L.; de la Torre, M.C.; Sierra, M.A. The organocatalytic desymmetrization of meso-ferrocene anhydride. *Tetrahedron Lett.* **2017**, *58*, 326–328. [CrossRef]
11. Butenschoen, H.; Werner, G. Improved Syntheses of 1,2-Disubstituted Ferrocenes. *Eur. J. Inorg. Chem.* **2017**, *2017*, 378–387.
12. Roling, P.V.; Rausch, M.D. Formation and characterization of 1,2-diiodoferrocene and related derivatives. *J. Org. Chem.* **1974**, *39*, 1420–1424. [CrossRef]
13. Wallace, C.E.; Selegue, J.P.; Carrillo, A. Synthesis and Characterization of a 1,2-Dibenzoylruthenocene and a Derived Pyridazine. *Organometallics* **1998**, *17*, 5146–5152. [CrossRef]
14. Tice, N.C.; Little, D.J.; Mattern-Mondragon, V.; King, S.T.; Selegue, J.P.; Parkin, S. Synthesis, Characterization, and Electrochemical Polymerization of Some 5,5-Fused Ring Terthiophene Tricarbonyl Manganese Complexes. *Organometallics* **2025**, *44*, 54–67.
15. Snyder, C.A.; Selegue, J.P.; Tice, N.C.; Wallace, C.E.; Blankenbuehler, M.T.; Parkin, S.; Allen, K.D.E.; Beck, R.T. Synthesis, Characterization, and Structure of Cyclopenta[c]thiophenes and Their Manganese Complexes. *J. Am. Chem. Soc.* **2005**, *127*, 15010–15011. [PubMed]
16. Snyder, C.A.; Tice, N.C.; Maddox, J.B.; Parkin, S.; Daniel, A.W.; Thomas, J.M. Synthesis, structure, and theoretical calculations of 1H-3,7-difurylcyclopenta[3,4-d]pyridazine. *Heterocycles* **2011**, *83*, 1275–1290. [CrossRef]
17. Pokharel, U.R.; Parkin, S.; Selegue, J.P. Synthesis and Structures of Ru(II)-*p*-Cymene Sandwich Complexes with Electron-Withdrawing Cyclopentadienyl Ligands. *Crystals* **2026**, *16*, 201.
18. Pokharel, U.R.; Selegue, J.P.; Parkin, S. Ruthenocene 1,2-Dicarboxylic Acid, Carboxylic Anhydride, and Acid Chloride: A Facile Route to Metallocene-Fused Acenequinones. *Organometallics* **2011**, *30*, 3254–3256. [CrossRef]
19. Quick, M.H.; Angelici, R.J. Pentacarbonylmanganese Halides. In *Inorganic Syntheses*; Angelici, R.J., Ed.; John Wiley & Sons: New York, NY, USA, 1990; Volume 28, pp. 154–159.
20. Fagan, P.J.; Ward, M.D.; Calabrese, J.C. Molecular engineering of solid-state materials: Organometallic building blocks. *J. Am. Chem. Soc.* **1989**, *111*, 1698–1719. [CrossRef]
21. Otwinowski, Z.; Minor, W. Processing of X-ray diffraction data collected in oscillation mode. *Methods Enzymol.* **1997**, *276*, 307–326. [CrossRef] [PubMed]
22. Bruker. *APEX2 Software Suite for Crystallographic Programs*; Bruker AXS, Inc.: Madison, EI, USA, 2009.
23. Krause, L.; Herbst-Irmer, R.; Sheldrick, G.M.; Stalke, D. Comparison of silver and molybdenum microfocus X-ray sources for single-crystal structure determination. *J. Appl. Crystallogr.* **2015**, *48*, 3–10. [PubMed]
24. Parkin, S.; Moezzi, B.; Hope, H. XABS2: An empirical absorption correction program. *J. Appl. Crystallogr.* **1995**, *28*, 53–56. [CrossRef]
25. Sheldrick, G.M. A short history of SHELX. *Acta Crystallogr. A* **2008**, *64*, 112–122. [PubMed]
26. Sheldrick, G.M. Crystal structure refinement with SHELXL. *Acta Crystallogr. C* **2015**, *71*, 3–8. [CrossRef]
27. Wilson, A.J.C. (Ed.) *International Tables for Crystallography, Volume C: Mathematical, Physical and Chemical Tables*; Kluwer Academic Publishers: Dordrecht, The Netherlands, 1992.
28. Parkin, S.R. PrimeXP: Python Retro Interactive Model Editor (Inspired by) XP. 2026. Available online: https://xray.uky.edu/Resources/PrimeXP.html (accessed on 1 April 2026).
29. Macrae, C.F.; Sovago, I.; Cottrell, S.J.; Galek, P.T.; McCabe, P.; Pidcock, E.; Platings, M.; Shields, G.P.; Stevens, J.S.; Towler, M. Mercury 4.0: From visualization to analysis, design and prediction. *Appl. Crystallogr.* **2020**, *53*, 226–235. [CrossRef]
30. Theodorou, V.; Skobridis, K.; Tzakos, A.G.; Ragoussis, V. A simple method for the alkaline hydrolysis of esters. *Tetrahedron Lett.* **2007**, *48*, 8230–8233. [CrossRef]
31. Ando, W.; Furuhata, T.; Tsumaki, H.; Sekiguchi, A. Synthetic Application of Thiosilanes to Thioesters. *Chem. Lett.* **1982**, *11*, 885–886. [CrossRef]

Disclaimer/Publisher's Note: The statements, opinions and data contained in all publications are solely those of the individual author(s) and contributor(s) and not of MDPI and/or the editor(s). MDPI and/or the editor(s) disclaim responsibility for any injury to people or property resulting from any ideas, methods, instructions or products referred to in the content.